CHEMISTRY OF MATERIALS

Article

pubs.acs.org/cm

Joint Experimental and Computational ^{17}O and ^{1}H Solid State NMR Study of $Ba_2In_2O_4(OH)_2$ Structure and Dynamics

Rıza Dervişoğlu,[†,‡,∥] Derek S. Middlemiss,[†,‡] Frédéric Blanc,[‡,⊥] Yueh-Lin Lee,[§] Dane Morgan,[§] and Clare P. Grey*[,†,‡]

[†]Department of Chemistry, Stony Brook University, Stony Brook, New York 11794-3400, United States

[‡]Department of Chemistry, University of Cambridge, Lensfield Road, Cambridge CB2 1EW, U.K.

[§]Department of Materials Science and Engineering, University of Wisconsin, Madison, Wisconsin 53706, United States

Supporting Information

ABSTRACT: A structural characterization of the hydrated form of the brownmillerite-type phase $Ba_2In_2O_5$, $Ba_2In_2O_4(OH)_2$, is reported using experimental multinuclear NMR spectroscopy and density functional theory (DFT) energy and GIPAW NMR calculations. When the oxygen ions from H_2O fill the inherent O vacancies of the brownmillerite structure, one of the water protons remains in the same layer (O3) while the second proton is located in the neighboring layer (O2) in sites with partial occupancies, as previously demonstrated by Jayaraman et al. (*Solid State Ionics* **2004**, *170*, 25−32) using X-ray and neutron studies. Calculations of possible proton arrangements within the partially occupied layer of $Ba_2In_2O_4(OH)_2$ yield a set of low energy structures; GIPAW NMR calculations on these configurations yield ^{1}H and ^{17}O chemical shifts and peak intensity ratios, which are then used to help assign the experimental MAS NMR spectra. Three distinct ^{1}H resonances in a 2:1:1 ratio are obtained experimentally, the most intense resonance being assigned to the proton in the O3 layer. The two weaker signals are due to O2 layer protons, one set hydrogen bonding to the O3 layer and the other hydrogen bonding alternately toward the O3 and O1 layers. ^{1}H magnetization exchange experiments reveal that all three resonances originate from protons in the same crystallographic phase, the protons exchanging with each other above approximately 150 °C. Three distinct types of oxygen atoms are evident from the DFT GIPAW calculations bare oxygens (O), oxygens directly bonded to a proton (H-donor O), and oxygen ions that are hydrogen bonded to a proton (H-acceptor O). The ^{17}O calculated shifts and quadrupolar parameters are used to assign the experimental spectra, the assignments being confirmed by $^{1}H-^{17}O$ double resonance experiments.

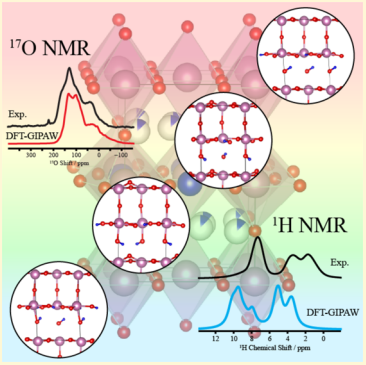

1. INTRODUCTION

Perovskites display a wide range of properties due to their ability to accommodate varying cations, substitutions, non-stoichiometry, and structural defects. They are consequently used in a widespread variety of applications. Of specific interest to this work is their application, when hydrated, as proton conductors at intermediate to high temperatures (above ca. 200 °C).[1,2] Initial studies by Iwahara et al. and Nowick et al. led to the discovery that perovskites such as $LaYO_3$,[3] $SrZrO_3$,[3] $SrCeO_3$,[4,5] $BaCeO_3$,[6,7] $KTaO_3$,[8] Sr_2GaNbO_6[9] and $Ba_3CaNb_2O_9$[10] have high proton conductivities under humid conditions. All of these materials require cation substitution in order to create oxygen vacancies and, upon hydration, the hydroxyl defects responsible for their proton conductivities. In contrast, $Ba_2In_2O_5$ is an inherently oxygen deficient perovskite, and hence cation substitution is not required to allow water uptake.

Compensation of the Ba^{2+} and In^{3+} cation charges in $Ba_2In_2O_5$ requires the removal of one-sixth of the O atoms in the perovskite structure, yielding a high intrinsic concentration of O vacancies along with both tetrahedrally and octahedrally coordinated In^{3+} ions. The vacancies order at room temperature into an orthorhombic structure, resulting in three crystallographically distinct O sites (Figure 1a). The labeling used here has O1 sites at the equatorial positions of In octahedra, O2 sites bridging In octahedra and tetrahedra and O3 sites within the In tetrahedral layer. We use this labeling scheme for both the dry and hydrated structures in contrast to some earlier work.[11,12] The structure type is named brownmillerite after the original Ca_2FeAlO_5 mineral which has a similar arrangement of O vacancies.[13] An understanding of the water uptake and protonic conduction processes in this system is of particular interest as the extremely large number of vacancies in the brownmillerite structure facilitates a level of hydration rarely possible in related materials.[14,15]

A TGA study of $Ba_2In_2O_5$ under wet air by Jayaraman et al.[11] found a maximum weight gain at around 200 °C, indicating the formation of the $Ba_2In_2O_4(OH)_2$ phase. Further heating results

Received: January 26, 2015
Revised: May 1, 2015
Published: May 1, 2015

DOI: 10.1021/acs.chemmater.5b00328
Chem. Mater. 2015, 27, 3861−3873

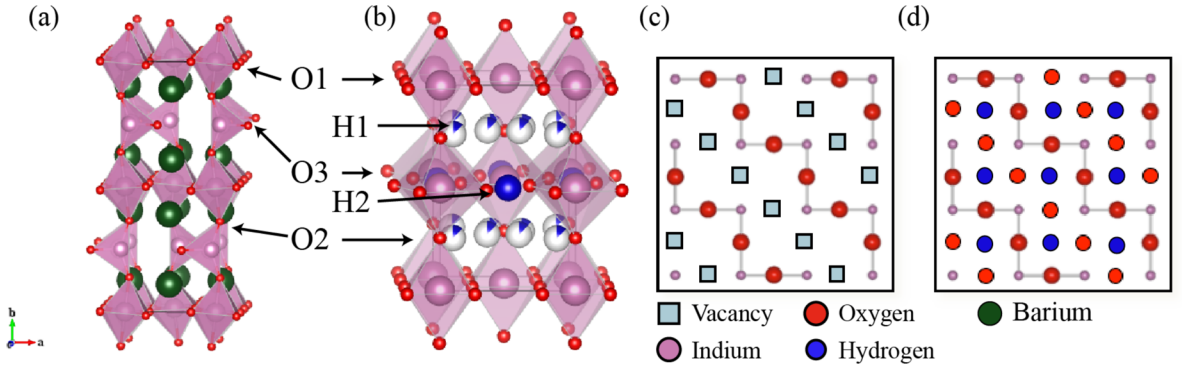

Figure 1. (a) Room temperature crystal structure of the brownmillerite $Ba_2In_2O_5$ structure in space group *Ibm*2[13,21] with an ···OctTetOctTet′··· staggered O vacancy pattern. (Reproduced from reference 22 by permission of the PCCP Owner Societies.) (b) Room temperature crystal structure of tetragonal $Ba_2In_2O_4(OH)_2$ in space group *P*4/*mbm*,[11] showing the partially occupied H1 and fully occupied H2 positions. Schematic representations of the O3 layer of (c) $Ba_2In_2O_5$ and (d) $Ba_2In_2O_4(OH)_2$. The interlayer Ba atoms in b, c, and d have been omitted for clarity. Sector filling of atoms in (b) denotes partial site occupancy.

in weight reduction due to H_2O loss, and a neutron powder diffraction study under controlled humid air by Yildirim et al.[16] showed that only $Ba_2In_2O_5$ is present above 350 °C. Studies by Schober et al.[17−19] and by Yildirim et al.[16] indicate that there is a metastable, partially hydrated $Ba_2In_2O_5$ phase (ca. 0.5 mol of H_2O per formula unit) with a slight deviation from the brownmillerite structure with the *Ima*2 space group. Complete hydration of $Ba_2In_2O_5$ results in a tetragonal structure with space group *P*4/*mbm* where the intrinsic O vacancies of $Ba_2In_2O_5$ in the O3 layer are fully occupied by the water O atoms, yielding the composition $Ba_2In_2O_5.H_2O$ (or $Ba_2In_2O_4(OH)_2$).[11,20] The 2*c* positions (in the O3 plane) are fully occupied by one of the water protons (H2) while the second proton (H1) partially occupies (12.5%) the 16*l* positions (in the O2 plane) according to the combined X-ray and neutron diffraction analyses of Jayaraman et al.[11] (Figure 1b). This model should be contrasted with that proposed in the earlier studies of Zhang and Smyth[23] where the water was believed to react with (O1) vacancies in the perovskite slabs, the vacancies resulting from p-doping and/or Frenkel defects created by occupancy of vacant O3 sites.

Early force field calculations of the energetics of defect formation by Fisher and Islam[20] questioned the role of the O1 vacancies proposed in the Zhang and Smyth model[23] and confirmed that the water oxygen atoms occupy the vacant O3 sites. They suggested, however, that the lowest energy site for the protons were the O1 sites. A subsequent DFT based, explicit full optimization of a large number of possible proton arrangements of the hydrated material $Ba_2In_2O_4(OH)_2$ (two formula units, i.e., 24 ions per unit cell) by Martinez et al.[12] identified a set of low energy structures with two protons (H2) in the O3 layer occupying half of the 4*h* (x, $\bar{x}$ + 0.5, 0.5) positions, and two other protons (H1) in one of the two O2 layers occupying one-16th of the 32*y* positions. The 32*y* positions are defined by Martinez et al.[12] and are derived from the 4*e* positions of the O2 site in the *P*4/*mbm* space group by the eight displacements (±0.4 Å, ±0.4 Å, ±0.4 Å). Note that this 32*y* position is not found in the International Tables for Crystallography[24] for the *P*4/*mbm* space group (No. 127) but it is nevertheless useful for visualization of the proton positions.

Zhang and Smyth[23] reported protonic conductivity of $Ba_2In_2O_4(OH)_2$ under humid air, where three regions of protonic conduction were observed corresponding broadly to temperatures below 400 °C, between 400 and 925 °C, and above 925 °C. These authors proposed both Grotthuss (H-hopping) and vehicle (OH-hopping) mechanisms as being involved in protonic conductivity: the Grotthuss mechanism dominating at low temperature; the vehicle mechanism or a combination of vehicle and Grotthuss mechanisms dominating at elevated temperatures.[23]

A study of $Ba_2In_2O_4(OH)_2$ and of its Ti-doped derivatives[11] using ^1H and ^2H solid state NMR experiments under magic angle spinning (MAS) identified three distinct proton sites (giving rise to a higher frequency split resonance and a lower frequency broad resonance), while only two proton sites are anticipated based upon the tetragonal crystal structure obtained by Jayaraman et al.[11] (Figure 1b). The increased splitting of proton sublattices in the NMR data as compared with the number of crystallographic sites found by neutron diffraction was interpreted as a result of a further ordering of proton sites with respect to the average structure. The authors postulated that this arises from the actual unit cell being larger than the average unit cell of the *P*4/*mbm* space group used in the refinement of the diffraction data (a larger cell having been observed in their electron diffraction studies), NMR being sensitive enough to distinguish between variations of different ordering schemes for at least one of the two environments. However, no clear assignments of these three proton resonances were given.

Our previous paper on $Ba_2In_2O_5$ focused on the dry material and used DFT methods to rationalize the ^{17}O spectra seen in this system.[22] The current work examines hydrated $Ba_2In_2O_5$ [i.e., $Ba_2In_2O_4(OH)_2$] using both current solid state ^{17}O and ^1H NMR spectroscopy techniques and DFT calculations. The DFT energetics and GIPAW calculations are first presented to describe the various configurations investigated in this work. We reproduce the general results of the DFT study by Martinez et al.,[12] although differences in the ground state structure and the energies of the other low energy structures are observed. First-principles periodic DFT NMR calculations within the gauge-including projector augmented wave (GIPAW) approach[25] are then performed to help interpret the NMR spectra. High magnetic field strengths are used to obtain NMR spectra of the hydrated material. This approach allows high resolution solid state NMR spectra of quadrupolar nuclei (such as ^{17}O, spin I = 5/2) to be obtained. The individual ^{17}O and ^1H NMR shifts are assigned to specific oxygen and proton environments, the DFT results allowing us to assign the

DOI: 10.1021/acs.chemmater.5b00328
Chem. Mater. 2015, 27, 3861−3873

three ^{1}H NMR signals seen at room temperature to specific local environments. We show that multiple low energy structural configurations are responsible for the experimental ^{1}H NMR spectra. The ^{17}O NMR spectra well reproduced with these multiple configurations, allowing us to assign the proton donor and acceptor oxygens. Variable temperature ^{1}H NMR spectroscopy is then used to probe proton motion.

2. MATERIALS AND METHODS

2.1. Experimental Methods. *2.1.1. Sample Preparation.* $Ba_2In_2O_5$ was prepared according to a literature procedure.[22] $Ba_2In_2O_4(OH)_2$ was prepared by slow cooling of $Ba_2In_2O_5$ (dried at 400 °C under a flow of dry N_2 for 12 h) from 350 °C to room temperature (at a rate of 0.1 °C.min^{-1}) under a flow of wet N_2 gas. The water vapor pressure corresponds to ∼20−30 mbar P_{H_2O} (∼2.3% (w/v) H_2O) and was controlled by bubbling N_2 through water at room temperature.[17] ^{17}O enriched $Ba_2In_2O_4(OH)_2$ was synthesized by heating previously synthesized $Ba_2In_2O_4(OH)_2$ in a 50% ^{17}O enriched O_2 gas (Isotec, used as received) atmosphere with ∼2.3% (w/v) H_2O (nonenriched) in a closed quartz tube, at 1000 °C for 24 h. During ^{17}O enrichment with the closed quartz tube, the initial air inside the tube was removed by vacuum while concurrently freezing the H_2O inside the tube with liquid N_2.

Powder X-ray diffraction patterns were obtained on either a Panalytical Empyrean or Bruker D8-Focus X-ray diffractometer using Cu Kα radiation (λ = 1.5418 Å; Figure S1 in the Supporting Information). Thermogravimetric analyses (TGA) were performed on a Mettler Toledo TGA/SDTA851 thermobalance using an alumina crucible (Supporting Information Figure S2). All measurements were performed under flowing dry nitrogen, in a temperature range of 30−800 °C and at a heating rate of 10 °C·min^{-1}. TGA showed that both $Ba_2In_2O_4(OH)_2$ and ^{17}O enriched $Ba_2In_2O_4(OH)_2$ contain 1 mol of water per formula unit, as anticipated.

2.1.2. Solid State NMR Spectroscopy. Solid state ^{17}O MAS NMR experiments on $Ba_2In_2O_4(OH)_2$ were performed on 9.4 T Bruker Avance 400 MHz and 16.4 T Bruker Avance III 700 MHz spectrometers using Bruker 2.5 mm HX probe and Bruker 3.2 mm HXY (in double resonance mode) probe, respectively. Unless otherwise stated, spectra were recorded using a solid ∼π/2 pulse length of 1 μs, corresponding to a radio frequency (rf) field amplitude of ∼83 kHz, and a MAS frequency of 30 kHz at 9.4 T, and a solid ∼π/2 pulse length of ∼1.7 μs, corresponding to a rf field amplitude of ∼50 kHz, and a MAS frequency of 20 kHz at 16.4 T. The ^{17}O 3QMAS experiment was performed at 9.4 T with 128 t_1 increments of 1320 scans each. Hard and soft pulses are performed at rf fields of 150 and ∼10 kHz, respectively. The ^{1}H−^{17}O cross-polarization (CP) and heteronuclear correlation (HETCOR)[26−29] spectra were obtained at 16.4 T with a ^{17}O rf field amplitude of ∼50 kHz, while the ^{1}H rf field amplitude was ramped to obtain maximum signal at ∼83 kHz. Small phase incremental alternation with 64 steps (SPINAL64)[30] ^{1}H heteronuclear decoupling was applied during the acquisition. Contact times for the CP experiments ranged between 5 and 5120 μs. All ^{17}O NMR data were collected on a freshly ^{17}O enriched $Ba_2In_2O_4(OH)_2$ sample packed in a ZrO_2 rotor. A recycle delay of 10 s was used for all experiments, with 20480 scans for ^{17}O Hahn-echo experiments and 48 t_1 increments of 256 scans for the HETCOR spectra.

^{1}H MAS NMR experiments were performed on a 16.4 T Bruker Avance III 700 MHz spectrometer equipped with a Bruker 4 mm HXY probe (in double resonance mode). One dimensional (1D) spectra were recorded under MAS using a rotor-synchronized spin echo sequence to suppress the proton background of the probe.[31] All ^{1}H spectra were recorded at a rf field amplitude of 100 kHz and a MAS frequency of 12.5 kHz with recycle delays ranging from 4 to 60 s depending on the T_1 relaxation times. Temperature calibration was performed using the ^{207}Pb resonance of $Pb(NO_3)_2$ as a chemical shift thermometer.[32,33] The sample temperatures quoted subsequently have all been corrected and have an accuracy of ±10 °C. Additional fast MAS ^{1}H NMR experiments were recorded on the same spectrometer with a Bruker 1.3 mm HX probe spinning at 60 kHz, using a rotor-synchronized spin echo sequence, an rf field amplitude of 115 kHz, and recycle delay of 8 s.

^{17}O and ^{1}H chemical shifts were externally referenced to water at 0.0 and 4.8 ppm, respectively, at 20 °C. NMR data were processed using TopSpin 3.0[34] and MatNMR,[35] the latter running within the MATLAB package. Simulations and deconvolutions were performed using the same software and SIMPSON.[36]

2.2. Computational Methods. *2.2.1. Energetics and Configurations.* The first-principles solid state electronic structure calculations used here are similar to those reported in our previous work on $Ba_2In_2O_5$ and in related studies[37−43] and were all performed within the CASTEP code.[44] Structural models of $Ba_2In_2O_4(OH)_2$ were derived, as described later, from the experimental neutron diffraction model by Jayaraman et al.[11] following the approach of Martinez et al.[12] Full structural optimizations (both cell and atomic positions) of $Ba_2In_2O_4(OH)_2$ (two formula units) were performed in the absence of any symmetry operators (i.e., in space group $P1$), using a plane wave kinetic energy cutoff of 40 Ry and a linear spacing of 0.04 Å^{-1} or smaller for the reciprocal space sampling mesh, yielding Monkhorst−Pack meshes of dimension 6 × 6 × 4 for the $Ba_4In_4O_8(OH)_4$ supercell. Full details of all of these structures are presented in the Supporting Information (SI). The Perdew−Burke−Ernzerhof GGA-type exchange-correlation functional has been used throughout.[45] Convergence of total energy with respect to numerical parameters was estimated at 0.2 kJ·mol^{-1} per atom or better. Structural optimizations (both cell parameters and atomic positions) pursued until the energy difference, maximum atomic force, maximum atomic displacement, and maximum stress tensor component fell below tolerances of 1 × 10^{-6} eV, 1 × 10^{-3} eV·Å^{-1}, 1 × 10^{-3} Å, and 5 × 10^{-3} GPa, respectively. The effect of decreasing these listed tolerances by a further order of magnitude was investigated, yielding only minimal changes in geometry and computed NMR parameters. To facilitate our exploration of the complex energy landscape, vibrational free energy contributions were not included in this analysis. However, given the relatively similar bonding sites being considered for the H, we assume that these contributions will largely cancel when comparing the relative energies. Previous work on a series of iron- and aluminum-oxyhydroxides calculated a less than 1.5 kJ/(mol of H) variation in vibrational free energies at room (25 °C) and synthesis (350 °C) temperatures for H across three compounds with both Fe and Al cations.[46,47] This error is as small or smaller than that found later between different DFT approaches, justifying exclusion of these contributions.

The hydration enthalpy of formation for the ground state configuration was calculated for the theoretical reaction of $Ba_2In_2O_5$ (staggered configuration)[22] with one isolated water molecule H_2O (calculated in a large unit cell with volume of 332 Å^3). DFT total energies of geometry-optimized structures were used in this calculation. The experimental enthalpy of hydration is reported to be −0.65 ± 0.08 eV (∼−63 kJ·mol^{-1}) with the Zhang−Smyth model and −0.76 eV (∼−74 kJ·mol^{-1}) (trapped) and −0.3 eV (∼−29 kJ·mol^{-1}) (untrapped) with the trapping model by Schober and Friedrich[18] at temperatures of 623−1073 K.

Boltzmann distribution weights at 350 °C were calculated according to $\text{weight}_i = (\exp(\Delta E_i/RT))/(\Sigma_i \exp(\Delta E_i/RT))$ where ΔE_i is the relative energy of a configuration from the ground state configuration, per mole of hydrogen. Structural models were visualized with the VESTA[48] and CrystalMaker packages.

2.2.2. NMR Calculations. Fully periodic calculations of NMR parameters within the gauge-including projector augmented wave (GIPAW) approach[25,49] have been performed using the CASTEP code, including determination of electric field gradient tensors and associated quadrupolar interaction parameters for ^{17}O sites.[50] The NMR parameters are obtained from single point calculations within the optimized geometry, differing only from the prior optimization runs in that a larger basis set cutoff of 60 Ry was applied. The isotropic shielding was obtained as $\sigma_{iso} = (\sigma_{xx} + \sigma_{yy} + \sigma_{zz})/3$, where σ_{xx}, σ_{yy}, and σ_{zz} are the principal components of the shielding tensor, ordered such that $|\sigma_{zz} - \sigma_{iso}| \geq |\sigma_{xx} - \sigma_{iso}| \geq |\sigma_{yy} - \sigma_{iso}|$. The chemical shift δ_{iso} is

DOI: 10.1021/acs.chemmater.5b00328
Chem. Mater. 2015, 27, 3861−3873

then derived from the computed site shielding σ_{iso} by application of a shielding reference σ_{ref} with the expression $\delta_{iso} = \sigma_{ref} + m\sigma_{iso}$. Both σ_{ref} and the scaling factor m for ^{17}O are taken unmodified from previous work by the current authors which obtained $\sigma_{ref} = 223.70 \pm 3.03$ ppm and $m = -0.888 \pm 0.014$ with a mean absolute error (MAE) in computed shifts relative to experiment of 12.1 ppm across a range of phases.[37] Meanwhile, σ_{ref} and m for ^{1}H are determined from a fit of the results of NMR CASTEP calculations on $Mg(OH)_2$ ($\sigma_{iso} = 30.89$ ppm; $\delta_{iso} = 0.5$ ppm)[51] in combination with 55 different proton sites in four separate organic molecules as computed recently by Yates et al.,[52] Webber et al.,[53] and Sardo et al.,[54] yielding $\sigma_{ref} = 28.45 \pm 0.51$ ppm and $m = -0.930 \pm 0.020$ with a MAE (defined similarly to those given earlier) of 0.29 ppm (SI Figure S3). We note that all but one of the proton sites used in deriving the shielding reference arise within organic molecules, and thus we might expect some discrepancy between experimental and calculated ^{1}H chemical shifts in $Ba_2In_2O_4(OH)_2$ as discussed later. Chemical shift anisotropies and asymmetries are also computed, defined as $\sigma_{aniso} = \sigma_{zz} - (1/2)(\sigma_{xx} - \sigma_{yy})$ and $\eta_{CS} = (\sigma_{yy} - \sigma_{xx})/(\sigma_{zz} - \sigma_{iso})$, respectively. The quadrupole coupling constant for ^{17}O is obtained as $C_Q = eQV_{zz}/h$ and the asymmetry as $\eta_Q = (V_{xx} - V_{yy})/V_{zz}$, where an ordering $|V_{zz}| \geq |V_{yy}| \geq |V_{xx}|$ of the principal components of the traceless electric field gradient tensor is assumed. The experimental value $Q = -0.02558$ barns has been used for the ^{17}O nuclear electric quadrupole moment.[55]

Unless otherwise specified, all of the corresponding simulated ^{17}O NMR spectra were obtained by simulation of each individual O site using SIMPSON[36] and summation of these spectra, resulting in the final spectra. No attempts were made to include $^{17}O-^{1}H$ dipolar couplings given that the spectra were acquired under MAS.

3. RESULTS AND DISCUSSION

3.1. DFT Energetics and Configurations. The structural optimization of $Ba_2In_2O_4(OH)_2$ was performed with the same approach as that used for $Ba_2In_2O_5$ in our previous work[22] taking the *P*4/*mbm* structure (Figure 1b) of Jayaraman et al. as the starting point.[11] The cell lengths of the *P*4/*mbm* cell are given by $\sqrt{2}a_p \times \sqrt{2}a_p \times 2a_p$ (where a_p is the notional perovskite unit cell length).[19,56] Sixteen arrangements of protons are considered. All structures feature full occupancy of the O3 layer proton positions (2*c* site) but have various proton configurations in the O2 (16*l* site with fractional occupancy of one-eigth; 14 arrangements) and O1 (two arrangements) layers, O1 occupancy not being observed by Jayaraman et al.[11] but identified theoretically by Fisher and Islam.[20] This results in configurations that are similar to those found in the study by Martinez et al.[12] The configurations are then ranked in terms of the calculated total energies (Figures 2 and 3 and Table 1). As was also shown by Martinez et al.,[12] all configurations undergo significant relaxations from the average positions suggested by Jayaraman et al.[11] The O2 layer protons (H1) move off the 16*l* positions [with fractional coordinates (*x*, *y*, 0.25)] suggested by neutron diffraction[11] into the "32*y*" positions (with values close to $x \pm 0.07$, $y \pm 0.07$, 0.25 ± 0.04, e.g., with $x = 0.10$, $y = 0.13$) retaining the nomenclature previously used by Martinez et al.[12] The computationally relaxed ground state forms alternating layers of ···O2−O3−O2−O1··· oxygens, partially occupied, fully occupied, non-occupied, and nonoccupied by protons, respectively (Figure 2b). Thus, the O3 layer O vacancies of $Ba_2In_2O_5$ are fully occupied by a hydroxyl group (Figures 1c and 2d), while the second water proton occupies one of the two nearby O2 layers. However, only one of the O2 layers is protonated, while the other remains empty (Figure 2b). The optimized In−O3−In bond angles differ significantly from In−O1−In and In−O2−In, and thus O3 oxygen atoms are in a significantly different electronic environment (Table 1). Moreover, the bond length

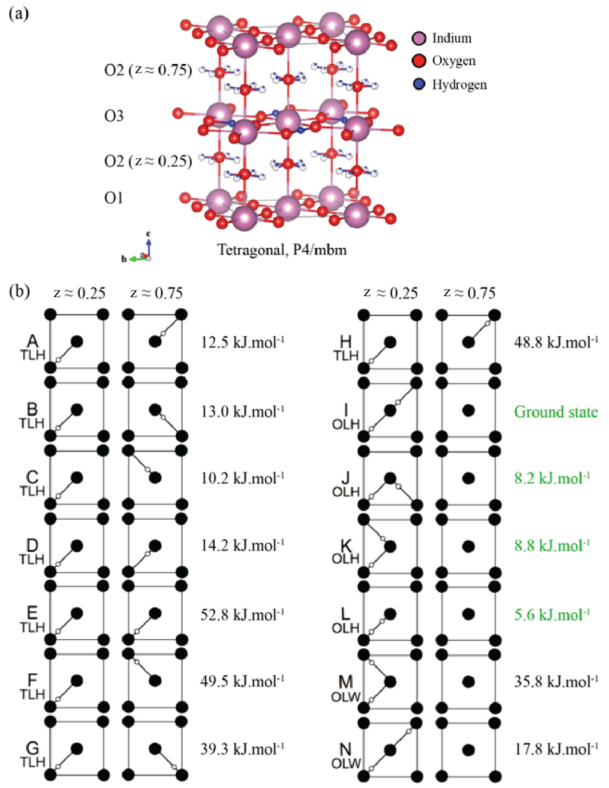

Figure 2. (a) Room temperature crystal structure of tetragonal $Ba_2In_2O_4(OH)_2$ in space group *P*4/*mbm*[11] showing full occupancy of the protons in the O3 layer (2*c* site) and partial occupancy in the O2 layer (16*l* site) (denoted, as in Figure 1b, by partially filled white balls). The interlayer Ba cations have been omitted for clarity. (b) Schematic representation of the 14 proton H1 configurations considered, differing in terms of the arrangement of protons in the O2 layers (16*l* site). Full and empty circles represent the O atoms and protons, respectively. Eight configurations (A−H) correspond to two-layer hydroxyl (TLH) forms; four configurations (I−L), to one-layer hydroxyl (OLH) forms; and two configurations (M−N), to one-layer water (OLW) forms. H1 protons were placed initially in the 16*l* positions with fractional occupancy of one-eighth determined by neutron diffraction,[11] and subsequently moved to the 32*y* positions on geometry optimization as in the previous study of Martinez et al.[12] The calculated energy per formula unit (containing two H atoms) of each configuration, relative to the ground state structure I, is also shown on the right-hand side of each configuration. A hydration enthalpy (ΔH_h) of −79.3 kJ·mol^{-1} to form the ground state configuration I from dry $Ba_2In_2O_5$ and a single molecule of H_2O was calculated. The hydration enthalpies of other configurations can be achieved by adding the relative energies to −79.3 kJ·mol^{-1}.

asymmetry of In−O2−In is substantial which may have implications for the ^{17}O NMR spectra of this phase (Table 1). The optimized structures also indicate that hydrogen bonding constitutes the main interaction driving the formation of a range of distinct chemical environments for both protons and oxygen ions.

The configurations were grouped into three different types. In the two-formula-units cell of $Ba_4In_4O_8(OH)_4$, two out of four protons are always in the O3 layer (H2) and the other two are each either in a different O2 layer (H1) [two-layer hydroxyl (TLH), configurations A−H], in the same O2 layer (H1) [one-layer hydroxyl (OLH), configurations I−L], or present as one water molecule (two protons attached to one oxygen) per layer [one-layer water (OLW), configurations M and N] (Figure 2).

DOI: 10.1021/acs.chemmater.5b00328
Chem. Mater. 2015, 27, 3861−3873

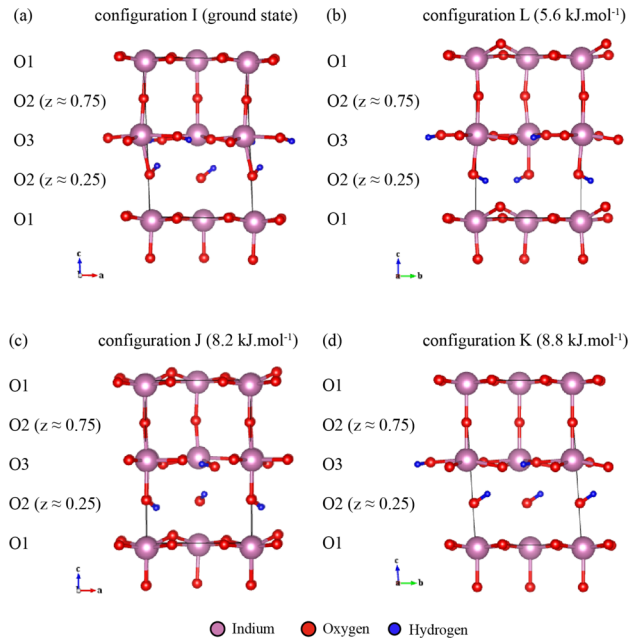

Figure 3. DFT optimized geometries of (a) configuration I (ground state), (b) configuration L, (c) configuration J, and (d) configuration K showing the O3 and O2 ($z \approx 0.25$ and 0.75) layer protons. The interlayer Ba atoms have been omitted for clarity.

OLH configuration I represents the ground state structure (with hydration enthalpy, $\Delta H_h = -79.3$ kJ·mol^{-1}) in which the protons in the O2 layer (H1) point toward two different O3 acceptors. Configurations in which the protons are located within one O2 layer (H1) (OLH, E_{ref} = 0−8.8 kJ·mol^{-1}) are systematically lower in energy than the OLW (E_{ref} 17.8 and 35.8 kJ·mol^{-1}) and TLH (E_{ref} = 10.2−48.8 kJ·mol^{-1}) arrangements. Here all energies are given as E_{ref} to denote their being referenced to the energy of the ground state structure I. All of the OLW configurations considered are unstable, configuration M relaxing to a mixed O1 and O2 layer protonation and configuration N to an OLH configuration. Structures where a proton is located in the O1 plane are noticeably higher in energy. For example, two configurations were also considered where the O3 layer is fully protonated and one O2 site and one O1 site are also protonated, the two structures differing in the relative orientations of the O1 and O2/O3 protons. Both of these structures are much higher in energy, occurring at 34.6 and 48.3 kJ·mol^{-1} above the ground state structure. The protons in both of these structures are located within the plane of the O1/In layers, in contrast with the structures proposed by Fisher and Islam[20] in which the O1−H bonds were oriented perpendicular to the plane.

Note that the previous study of Martinez suggested the present configuration L as the ground state structure (first low energy state), in which the O2 layer protons point toward the O1 oxygen site (Figures 2b and 3); a structure close to configuration I represented their first excited state.[12] The fact that the present and the Martinez et al. studies[12] disagree on the energy ordering of structures at the ∼6 kJ·mol^{-1} (or just ∼3 kJ/(mol of H)) level suggests that the DFT approach used cannot be regarded as yielding energies any more accurately than to within a few kJ/(mol of H). Thus, it is clear that we should consider more than just the ground state structure when analyzing our NMR data. Bielecki et al.,[57] in an inelastic neutron scattering (INS) study of hydrogen bonding in this material, suggested that the second lowest energy structure of Martinez et al.[12] should not exist due to its strong hydrogen bonds, which would result in higher frequency O−H wag modes than observed experimentally. However, our related structure (ground state structure I) has a longer hydrogen bond distance (1.819 Å; see Table 1) than that obtained by Martinez et al.[12] (1.7 Å). Hence, structure I is likely consistent with the lower frequency O−H wag modes observed experimentally and cannot be ruled out on the basis of the INS data.

The thermal energy $k_B T N_A$ (or RT) at a typical hydration synthesis temperature (350 °C) is ∼5 kJ. Assuming fast cooling (equilibrium of atomic motion is not reached in the given time frame and temperature), this suggests that configurations with up to ∼5 kJ/(mol of H) may be present at significant concentrations at room temperature. We note that H is quite mobile in this system. A previous thermogravimetric study of hydrated $Ba_2In_2O_5$ by Schober and Friedrich[18] suggests an activation energy of 0.3 eV (∼30 kJ·mol^{-1}) for trapping effects in the hydration, as well as a hydrogen diffusion enthalpy (ΔH^*) of 0.34 eV with diffusion coefficient prefactor (D_0) of 0.34×10^{-5} cm^2/s. These values all suggest that at least some H can readily diffuse at room temperature (as will be explored later by ^{1}H NMR spectroscopy). However, we propose that either some of the H^+ ions are significantly less mobile or that the cooperative motion of the H needed to reorder is inhibited, despite the good mobility of individual H^+ ions. We therefore consider GIPAW calculations on the first four lowest energy structures I, J, K, and L, all of which are of OLH-type and have relative energies in the range of 0−8.8 kJ·mol^{-1} (or 0−4.4 kJ/(mol of H)), consistent with the possibility of thermal excitations being trapped in the system and the uncertainty in DFT energies and neglected vibrational energies mentioned earlier. We also limit ourselves to these four structures as they are clearly distinct in character from the next highest energy structures C, A, and B [at 10.2, 12.5, and 13.0 kJ·mol^{-1}, respectively (or ∼6 kJ/(mol of H))], which all have protons in both O2 layers (z = 0.25 and 0.75).

Assuming all of the structures occur with a Boltzmann distribution established at 350 °C, the relative amounts of each configuration are given by the Boltzmann weights 0.25, 0.11, 0.11, and 0.15 for I, J, K, and L, respectively, and 0.09, 0.08, 0.07, 0.06, and 0.05 for the configurations C, A, B, D, and N, respectively; the remaining seven configurations have weights of less than 0.01 contributing total weights of approximately 0.02. We discuss the preceding assumptions in the context of the NMR experiments.

3.2. Experimental and GIPAW Calculations Results.

3.2.1. X-ray Powder Diffraction. The X-ray powder diffraction pattern of $Ba_2In_2O_4(OH)_2$ samples and the ^{17}O enriched counterpart prepared in this study are consistent with previous reports[11,19] (Figure S1 in the Supporting Information) and indicate that the structure has tetragonal $P4/mbm$ symmetry.[11]

3.2.2. ^{17}O NMR Spectroscopy. The 1D ^{17}O MAS NMR spectrum of ^{17}O enriched $Ba_2In_2O_4(OH)_2$ obtained at 9.4 T under conditions where the line shape distortion is minimal (i.e., with short pulse length)[58] shows a complicated pattern characteristic of multiple overlapping ^{17}O resonances (Figure 4). Four sites could be resolved in the ^{17}O 3QMAS experiment (Figure 5), which could be satisfactorily fit with the NMR parameters given in Table 2. Fitting of the 1D ^{17}O MAS NMR spectra with these parameters yields an intensity ratio of 4:1:6:4 for the resonances with chemical shifts of 188, 173, 152, and 97 ppm, respectively (Figure 4). In addition to these resonances

DOI: 10.1021/acs.chemmater.5b00328
Chem. Mater. 2015, 27, 3861−3873

Table 1. Cell Constants (a, b, and c, Å; α, β, and γ, deg), In−O and O−H Bond Distances (Å) and In−O−In and O−H···H Bond Angles (deg) for O1, O2, and O3 Environments Obtained from Optimizations of the Initial Perturbed $P1$ Symmetry $Ba_4In_4O_8(HO)_4$ Cells, in the Lowest Energy I, J, K, and L Configurations (Figure 2b), As Compared with Corresponding Experimental and Calculated Literature Values[a]

	present calculations						
	I struct ($P1$)	J struct ($P1$)	K struct ($P1$)	L struct ($P1$)	average of I, J, K, and L structures	calculations Martinez et al.[12]	experimental Jayaraman et al.[11] ($P4/mbm$)
cell							
a (Å)	5.975	5.951	5.929	5.966	5.955(0.017)		5.915
b (Å)	5.992	6.029	5.984	5.979	5.996(0.020)		5.915
c (Å)	9.308	9.225	9.324	9.247	9.276(0.041)		8.999
α (deg)	93.3	87.9	93.7	89.7	91.2(2.4)		90
β (deg)	93.1	90.2	90.0	90.0	90.8(1.3)		90
γ (deg)	90.3	91.0	90.0	92.1	90.8(0.8)		90
In−O1−In							
distance (Å)	2.120 (0.006)	2.138 (0.014)	2.112 (0.006)	2.160 (0.023)	2.133 (0.028)		2.092*
	2.132 (0.008)	2.162 (0.008)	2.121 (0.001)	2.162 (0.024)	2.144 (0.026)		2.092*
angle (deg)	169.1 (2.5)	164.0 (11.0)	168.5 (1.3)	160.4 (14.8)	165.5 (18.7)		178.4
In−O2−In							
distance (Å)	2.274 (0.162)	2.251 (0.138)	2.299 (0.183)	2.213 (0.076)	2.259 (0.290)		2.192*
	2.411 (0.231)	2.391 (0.235)	2.378 (0.172)	2.428 (0.250)	2.402 (0.448)		2.307*
angle (deg)	173.9 (4.1)	169.6 (5.9)	175.6 (3.1)	170.9 (1.7)	172.5 (8.0)		180.0
In−O3−In							
distance (Å)	2.231 (0.067)	2.245 (0.085)	2.250 (0.053)	2.253 (0.080)	2.244 (0.145)		2.201
	2.293 (0.108)	2.297 (0.128)	2.274 (0.064)	2.262 (0.087)	2.282 (0.199)		2.201
angle (deg)	139.0 (4.4)	138.1 (1.2)	137.5 (3.7)	139.2 (6.0)	138.4 (8.4)		143.6
O3−H···O							
distance (Å)	1.011 (0.005)	1.013 (0.001)	1.022 (0.000)	1.018 (0.002)	1.016 (0.006)		1.404
	1.750 (0.035)	1.720 (0.020)	1.676 (0.000)	1.680 (0.037)	1.707 (0.055)	1.7	1.404
angle (deg)	173.3 (5.3)	175.3 (0.2)	177.8 (0.0)	176.7 (0.5)	175.8 (5.3)		180.0
O2−H···O							
distance (Å)	0.993 (0.003)	0.983 (0.001)	0.995 (0.000)	0.982 (0.001)	0.988 (0.003)	1.00*	0.991 (0.000)*
	1.819 (0.005)	1.969 (0.005)	1.844 (0.000)	1.957 (0.014)	1.897 (0.016)	1.90	2.542 (0.051)
angle (deg)	153.5 (1.8)	151.0 (1.7)	154.5 (0.0)	150.0 (1.7)	152.2 (3.0)		116.4 (4.2)

[a]Means and standard deviations (in parentheses) of the values are shown. For values marked with an asterisk (*), note that the O1 and O2 labels of the Jayaraman et al. structure are switched in order to match this work and the previous publication on the $Ba_2In_2O_5$ phase.[22]

there is a fifth peak at 220 ppm which nutates at the same frequency as water (i.e., it must be associated with a very small or zero quadrupolar coupling) and is tentatively attributed to either a possible H_2O molecule on the surface of the material as also discussed in our previous paper,[22] or to an impurity phase. The ^{17}O signals in the 3QMAS show a broadening along the +1 direction (positive slope diagonal), which is attributed to a distribution of chemical shifts arising from a distribution of different local environments.

The ^{17}O isotropic chemical shifts, δ_{iso}, obtained by GIPAW calculations of the lower energy I, J, K, and L structures of $Ba_2In_2O_4(OH)_2$ are also given in Table 2 and are found to span a wide range of values for each O sublattice O1, O2, and O3 (Figure 6). Nevertheless, we may divide the sites into three general types of oxygen atoms, namely, bare oxygens (O), oxygens directly bonded to a proton (H-donor O), and oxygen ions that are hydrogen bonded to a proton (H-acceptor O).

More specifically, we note that O1, H-acceptor O1, O2, H-donor O2, H-donor O3, and H-acceptor O3 local environments occur in all of the low energy structures I, J, K, and L (see Table 2). A range of C_Q are also observed, where C_Q for the H-acceptor O sites ranges from 3.8 to 4.5 MHz, the H-donor O sites from 5.3 to 6.9 MHz, and the bare O sites from 4.9 to 5.5 MHz. Two distinct ranges for the quadrupolar asymmetry parameter η_Q are obtained: those for bare O sites are approximately 0.1, while those for H-donor and -acceptor O sites are approximately 0.7. Taking the ground state structure I as an example, the O1 (sites 1−4 in Figure 6a, δ_{iso} = 170.4 ppm), O2 (sites 5 and 8 in Figure 6a, δ_{iso} = 159.6 ppm), and H-acceptor O3 (sites 9 and 12 in Figure 6a, δ_{iso} = 156.4 ppm) all contribute to the high frequency resonances in the experimental spectrum (mean, 164 ppm), while the H-donor O2 (sites 6 and 7 in Figure 6a, δ_{iso} = 114.4 ppm) and H-donor O3 (sites 10 and 11 in Figure 6a, δ_{iso} = 94.5 ppm) contribute to the lower frequency resonances (mean, 104 ppm) (see Table 2).

$^1H-^{17}O$ double resonance experiments probe the $^1H-^{17}O$ heteronuclear dipolar coupling (and hence the $^1H-^{17}O$ heteronuclear distance) and were therefore carried out to investigate the spatial proximities between the ^{17}O sites and protons. The ^{17}O cross-polarization (CP) spectrum of ^{17}O enriched $Ba_2In_2O_4(OH)_2$ recorded with a very short contact time (τ_{CP} = 40 μs) is given in SI Figure S4b and reveals a single resonance corresponding to the low frequency signal at δ_{iso} = 97 ppm, confirming its assignment to H-donor oxygens. Additionally, a two-dimensional $^1H-^{17}O$ heteronuclear corre-

DOI: 10.1021/acs.chemmater.5b00328
Chem. Mater. 2015, 27, 3861−3873

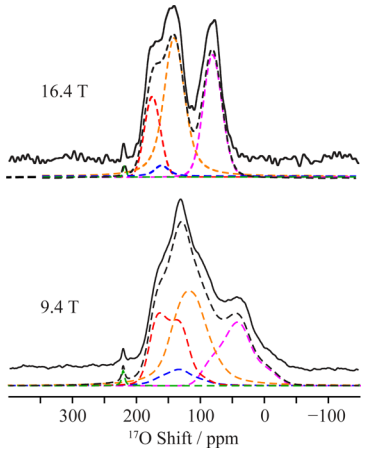

Figure 4. ^{17}O MAS NMR spectra of ^{17}O enriched $Ba_2In_2O_4(OH)_2$ obtained at 9.4 and 16.4 T. Experimental spectra are shown with full lines and total best-fit simulations in black dashed lines. The individual site components are shown as dashed lines in red (site A, O1), blue (site B, acceptor O1), orange (site C, combination of acceptor O2 and acceptor O3), pink (site D, donor O2 and donor O3), and green (small quadrupole coupling impurity site) (see Table 2). Assignments of the O sites are made by comparison with parameters derived from DFT GIPAW calculations (see Figure 6).

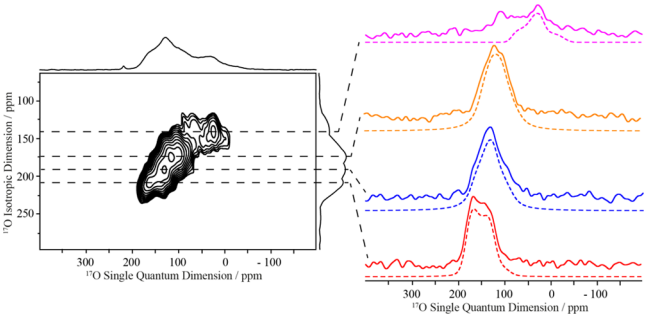

Figure 5. Two-dimensional ^{17}O 3QMAS spectrum of ^{17}O enriched $Ba_2In_2O_4(OH)_2$ obtained at 9.4 T. Right: experimental cross-sections (full lines) obtained at δ_1 = 140 (pink), 174 (orange), 192 (blue), and 207 ppm (red) along with best-fit simulations (dashed lines) using the parameters given in Table 2. The weaker high frequency component in the δ_1 = 140 (pink) slice results from an overlap with the more intense resonances with larger δ_1 values (as explained in the main text) and has thus not been included in the line-shape simulation.

lation (HETCOR) spectrum, also recorded with τ_{CP} = 40 μs, shows that this 97 ppm resonance correlates with all of the ^{1}H signals (see SI Figure S4a and section 3.2.3). The ^{17}O CP spectrum obtained with a longer contact time of 2.5 ms (SI Figure S4b) still does not contain the signals observed at high frequencies (δ_{iso} = 188 and 173 ppm) in the ^{17}O MAS spectrum (Figure 4), indicating that the O sites that give rise to these resonances are not in close proximity to the protons (or that the associated protons are too mobile). Instead a weak resonance at δ_{iso} = 152 ppm is observed which is tentatively assigned to an H-acceptor oxygen. The ^{17}O CP kinetics curve (SI Figure S5) shows the slower CP dynamics associated with the 152 ppm compared to the 97 ppm resonance, consistent with our assignment of the 152 ppm resonance to a H-acceptor O site.

Assuming that all of the low energy configurations, I, J, K, and L contribute to the spectrum with weights from the Bolztmann distribution at 350 °C (given by 0.25, 0.11, 0.11, and 0.15, respectively), we combined all of the oxygen resonances obtained from the GIPAW calculations to yield the simulated spectra shown in Figure 6b. A peak intensity ratio of 4.3:1:6.3:4.3 (from high to low frequency) is derived, which is remarkably close to the experimentally derived 4:1:6:4 ratio. On the basis of this reasonable agreement, the experimentally observed high frequency resonance at δ_{iso} = ∼188 ppm is, therefore, assigned to the bare O1 sites; the other high frequency weaker resonance at 173 ppm, to the acceptor O1 sites; the next resonance at δ_{iso} = ∼152 ppm, to the bare O2 sites and H-acceptor O3 sites; and finally the lowest frequency resonance at δ_{iso} = ∼97 ppm, to the H-donor O2 and H-donor O3 sites, in agreement with the ^{17}O CP experiments, all of these sites corresponding to the 48 O sites in the four $Ba_4In_4O_8(OH)_4$ configurations, I, J, K, and L (Figure 3 and Table 2). In summary, the present first-principles calculations permit the assignment of the ^{17}O MAS NMR spectrum of $Ba_2In_2O_5(OH)_2$, yielding chemical shifts and quadrupolar parameters in reasonable agreement with the experimental trends, albeit with some minor differences in the chemical shifts, quadrupolar parameters, and relative resonance intensities. A likely source of error in the intensities is the assumption that only structures I, J, K, and L contribute to the experimental spectra in proportions governed by their relative energies and the synthesis temperature. However, the assignment of the "high" and "low" shift peaks in the ^{17}O MAS NMR experimental spectra is consistent; i.e., we expect nondonor oxygen resonances to occur in the high frequency region and a donor oxygen to occur in the low frequency region. Overall, while relative intensities of the experimental peaks may vary, their assignment to these chemical environments is sound.

3.2.3. ^{1}H NMR Spectroscpy. The room temperature ^{1}H MAS NMR spectrum of $Ba_2In_2O_4(OH)_2$ obtained at 16.4 T clearly shows three distinct proton sites at shifts of 7.3, 3.3, and 1.7 ppm in a 2:1:1 intensity ratio (Figure 7). ^{1}H/^{2}H NMR resonances in approximately the same chemical shift range were observed by Jayaraman et al.[11] in their study of this material; however, these authors observed a splitting of the higher frequency resonance (of approximately 1−2 ppm), a broader resonance being observed at lower frequencies (at approximately 2.5 ppm) and the high (split) and low frequency resonances occurring with intensity ratios of 1:1. No assignment was given in that study. The three resonances observed in our study are fairly broad, and we assign this to inhomogeneous broadening (i.e., a chemical shift distribution) rather than to the effects of strong homogeneous dipolar interactions between protons, as similar ^{1}H line widths were obtained in spectra acquired under fast MAS conditions (SI Figure S6).[59]

In order to assign all three resonances observed in the experimental ^{1}H MAS NMR spectrum of $Ba_2In_2O_4(OH)_2$, we computed the ^{1}H site shielding tensors in the proton arrangements discussed earlier (Table 2 and Figure 7 and SI Figure S7). A simulation of the ^{1}H spectrum using the calculated NMR parameters (SI Figure S7) of the lowest energy structure I contains three peaks with a 1:1:2 ratio (∼9, ∼8, and ∼5 ppm), providing a poor match with the experimental spectrum (Figure 7a). Thus, in order to generate a spectrum that is closer to the experimental one, other low energy structures were also considered. Inclusion of the first high energy configuration (L; with Boltzmann weights of 0.25 and 0.11 for I and L) improves the fit to the spectrum in the low part per million region but worsens it in the higher frequency

DOI: 10.1021/acs.chemmater.5b00328
Chem. Mater. 2015, 27, 3861−3873

Table 2. Experimental and Calculated ^{1}H and ^{17}O Isotropic Shift (δ_1, ppm), Isotropic Chemical Shift (δ_{iso}, ppm), Quadrupolar Coupling Constant (C_Q, MHz), and Quadrupolar Asymmetry Parameter (η_Q) for $Ba_2In_2O_4(OH)_2$

structure	nucleus	environment[a]	δ_1 (ppm)	δ_{iso} (ppm)	C_Q (MHz)	η_Q[b]	N[c]
			Experimental[d]				
$Ba_2In_2O_4(OH)_2$	^{17}O	O-site A (O1)[a]	140	188(4)	4.5(2)	0.0(1)	0.25
	^{17}O	O-site B (H-acc. O1)[a]	174	173(4)	4.1(2)	0.7(1)	0.0625
	^{17}O	O-site C (H-acc. O2 and O3)[a]	192	152(4)	4.2(2)	0.5(1)	0.375
	^{17}O	O-site D (H-donor O2 and O3)[a]	207	97(4)	4.8(2)	0.7(1)	0.25
	^{17}O	O-site E (no match)		223(4)	1.0(2)	0.0(1)	0.0625
	^{1}H	H-site A (H2, O3 plane)[a]		7.3(1)			0.5
	^{1}H	H-site B (H1, O2 plane I,K)[a]		3.3(1)			0.25
	^{1}H	H-site C (H1, O2 plane J,L)[a]		1.7(1)			0.25
			Calculated[b]				
I	^{17}O	O1	200.6 (11.1)	170.4 (7.0)	−5.0	0.2	0.33
	^{17}O	donor O2	168.7 (5.2)	114.4 (3.3)	−6.0	0.8	0.167
	^{17}O	O2	193.4 (1.1)	159.6 (0.7)	−5.3	0.1	0.167
	^{17}O	donor O3	136.9 (1.6)	94.5 (1.0)	5.3	0.8	0.167
	^{17}O	acceptor O3	180.0 (19.7)	156.4 (12.4)	−4.3	0.5	0.167
	^{1}H	H2, O3 plane		8.5 (0.7)			0.5
	^{1}H	H1, O2 plane		5.3 (0.1)			0.5
J	^{17}O	O1	217.7 (11.3)	185.1 (7.1)	−5.2	0.2	0.25
	^{17}O	acceptor O1	204.6 (0.0)	175.4 (0.0)	−4.4	0.8	0.083
	^{17}O	donor O2	167.0 (10.2)	103.6 (6.4)	−6.9	0.6	0.167
	^{17}O	O2	204.2 (9.8)	169.1 (6.2)	−5.4	0.1	0.167
	^{17}O	donor O3	149.6 (3.2)	107.0 (2.0)	5.1	0.9	0.167
	^{17}O	acceptor O3	185.7 (0.5)	158.5 (0.3)	−4.4	0.7	0.167
	^{1}H	H2, O3 plane		8.8 (0.3)			0.5
	^{1}H	H1, O2 plane		4.0 (0.2)			0.5
K	^{17}O	O1	197.5 (1.7)	168.5 (1.1)	−4.9	0.2	0.33
	^{17}O	donor O2	171.2 (0.0)	117.1 (0.0)	−6.2	0.7	0.167
	^{17}O	O2	200.2 (0.0)	166.5 (0.0)	−5.3	0.0	0.167
	^{17}O	donor O3	146.8 (0.0)	103.5 (0.0)	5.7	0.6	0.167
	^{17}O	acceptor O3	169.8 (0.0)	151.9 (0.0)	−3.8	0.4	0.167
	^{1}H	H2, O3 plane		9.7 (0.0)			0.5
	^{1}H	H1, O2 plane		5.1 (0.0)			0.5
L	^{17}O	O1	223.8 (19.1)	188.6 (12.0)	−5.4	0.2	0.25
	^{17}O	acceptor O1	225.4 (0.0)	196.9 (0.0)	4.5	0.7	0.083
	^{17}O	donor O2	166.7 (1.3)	105.1 (0.8)	−6.8	0.6	0.167
	^{17}O	O2	207.2 (5.6)	170.8 (3.5)	−5.5	0.1	0.167
	^{17}O	donor O3	142.8 (11.9)	98.8 (7.5)	5.4	0.8	0.167
	^{17}O	acceptor O3	178.1 (16.4)	154.0 (10.3)	−4.0	0.8	0.167
	^{1}H	H2, O3 plane		9.5 (0.4)			0.5
	^{1}H	H1, O2 plane		3.8 (0.1)			0.5

[a]An asterisk denotes the most plausible O and H environments from four hydrated models. Standard deviations are also given in parentheses; deviations of quadrupolar parameters C_Q and η_Q are less than 0.01 and are therefore omitted. [b]Obtained from the averaged DFT calculated NMR parameters of the four low energy structures I, J, K, and L. The calculated values of δ_1 are obtained with $\delta_1 = (27\delta_{iso} - 10\delta_2)/17$ with $\delta_2 = \delta_{iso} - (3/500)((C_Q^2(1 + \eta_Q^2/3))/\nu_0^2)$ for ^{17}O ($I = 5/2$) (see ref 58), the errors arising from the range of δ_{iso} values. [c]Molar fraction of the site in the structure specified. [d]Obtained from the 3QMAS and ^{1}H−^{17}O HETCOR experiments. δ_{iso} was determined from the center of gravity of each peak in F_2 (δ_2) and F_1 (δ_1) as $\delta_{iso} = (10/27)\delta_2 + (17/27)\delta_1$ and C_Q from the fit of the δ_2 cross-sections through the ridge line shapes.

region (Figure 7b). When all of the low energy configurations, with respective weights, are considered ($E_{ref} < 20$ kJ·mol^{-1}), we do not observe a narrow peak at the high shift region in the spectrum (Figure 7c). Concentrating on NMR parameters obtained in the four most stable configurations (structures I, J, K, and L), the calculations yield O3 layer proton resonances at δ_{iso} of 7.8−9.3 ppm (due to configuration I), 8.6−9.1 (configuration J), 9.7 (configuration K), and 9.1−9.9 ppm (configuration L) (Figure 7d; spectrum shown with 350 °C Boltzmann weights). In some proportion, all of these O3 layer ^{1}H signals are likely to contribute to the broad signal ($\Delta\nu_{1/2}$ = 800 Hz (∼1.5 ppm on 16.4 T magnet)) observed experimentally at approximately 7.3 ppm for $Ba_2In_2O_4(OH)_2$ (Figure 7a). Two distinct sets of shifts are observed, at 5.2 ± 0.2 ppm from the O2 layer protons (H1) in structures I and K and at 3.9 ± 0.2 ppm arising from structures J and L (Figure 7, Table 2), which are reasonably close to the two experimental resonances observed at 3.3 and 1.7 ppm.

Of note, the spectrum simulated with structure I resembles that obtained by Jayaraman et al.,[11] predicting the small

DOI: 10.1021/acs.chemmater.5b00328
Chem. Mater. 2015, 27, 3861−3873

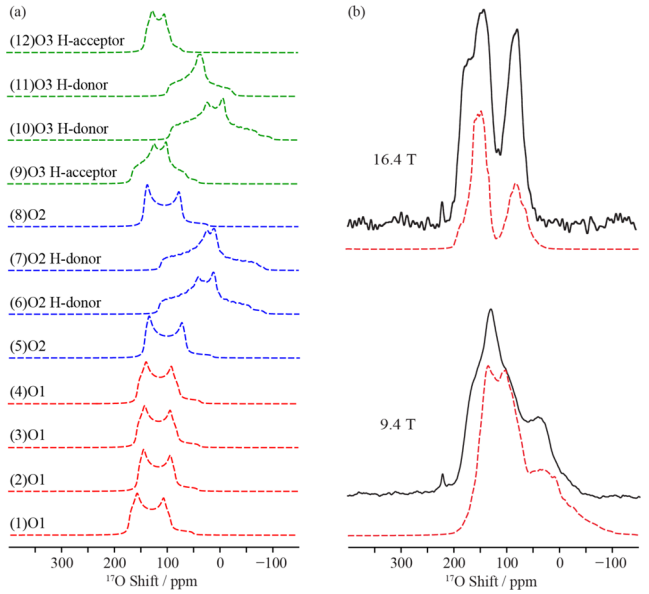

Figure 6. (a) Simulation of the GIPAW calculated ^{17}O NMR spectra of the 12 sublattice O sites occurring in the lowest energy optimized structure I of $Ba_2In_2O_4(OH)_2$. All of the spectra were simulated at 9.4 T. (b) Comparison of the experimental ^{17}O NMR spectra of ^{17}O enriched $Ba_2In_2O_4(OH)_2$ (black lines) and the sum of the simulation of the GIPAW calculated ^{17}O NMR spectra (dashed red lines) of all O sites of the four lower energy structures $Ba_2In_2O_4(OH)_2$ (I, J, K and L, combined with relative weights of 0.25, 0.11, 0.11 and 0.15) at 9.4 and 16.4 T.

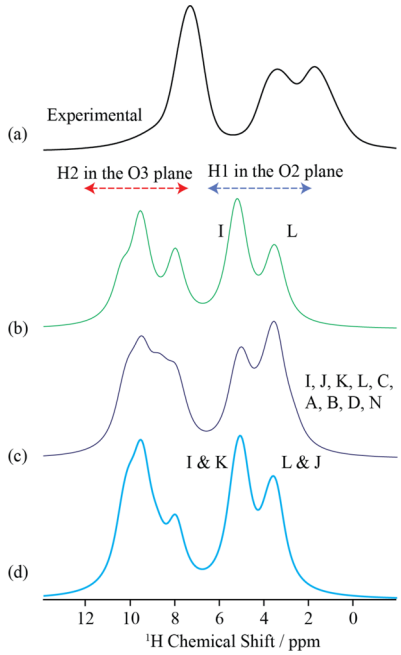

Figure 7. ^1H NMR spectrum of $Ba_2In_2O_4(OH)_2$: (a) experimental data, (b) simulation of combined GIPAW calculated parameters of structures I and L, (c) all structures with E_{ref} < 20 kJ·mol^{-1}, and (d) structures I, J, K, and L. The blue dashed line with double arrows indicates the 2–6 ppm region corresponding to the H1 protons in the O2 plane, and the red dashed line with double arrows indicates the 7–11 ppm region corresponding to the H2 protons in the O3 plane. Simulations are carried with a 0.8 ppm Lorentzian line broadening summing the spectra using the respective 350 °C Boltzmann weights for structures I and L in b; I, J, K, L, C, A, B, D, and N in c; and I, J, K and L in d.

splitting at higher frequency and the absence of a splitting at lower frequency. This may suggest that the sample prepared by these authors is more ordered than ours (i.e., contains fewer proton configurations), with a structure that is closer to that of the thermodynamic ground state.

The apparent offset in δ_{iso} between the calculated and experimental values for all of the structures and sites is relatively constant at approximately 2 ppm, a value larger than the ^1H calculated standard deviation of 0.29 ppm (see Computational Methods and SI Figure S3) and may be due to a systematic error in the ^1H shielding reference, arising out of the use of primarily organic phases in deriving σ_{ref}. More work is required to obtain a reliable set of reference parameters for protons in inorganic materials, preferably considering hydrated oxides and simple hydrous phases. In addition, proton motion and, likely, systematic deviation in calculated to experimental lattice constants may also play a role in the ^1H chemical shift. The fact that the protons are involved in chains of hydrogen bonding in the $Ba_2In_2O_4(OH)_2$ system means that the ^1H chemical shift will be very sensitive to lattice dilation/contraction. Nonetheless, the relative chemical shifts and relative intensities of the calculated resonances are in good agreement with experiment. Of note, the results show that configurations in which the O2 protons are involved in hydrogen bonds with *both* the O3 and O1 sublattices must be included in order to account for the split H1 (O2) resonance observed in our sample.

It is evident from the H···O (hydrogen bond) distances in Table 1 and the ^1H chemical shifts in Table 2 that longer hydrogen bonds result in a lower ^1H chemical shift. A study by Yesinowski et al.[60] on a series of hydrated silicates yielded an inverse correlation between donor O to acceptor O distance and ^1H chemical shift characterized by the following equation.

$$\delta_{iso}(\text{ppm}) = 79.05 - 25.5[d(\text{O}-\text{H}\cdots\text{O})/\text{Å}] \quad (1)$$

Applying this equation to the O–O distances from the I, J, K, and L structures, we calculate ^1H shifts of 7.4 and 9.7 ppm for O2 and O3 layer protons, respectively. Slightly better fits to experiment were obtained by using the empirical equations derived by Xue and Kanzaki for a wider range of hydrous silicates and related inorganic materials (yielding 5.5 and 8.0 ppm for the O2 and O3 layer protons).[61] These simple calculations provide trends and allow us to distinguish the O3 and O2 layer protons from each other, but do not provide the ability to further separate the two types of O2 layer protons. The predicted shifts are noticeably larger than those observed experimentally, particularly for the O2 coordinated protons, most likely due the very different systems studied here than used to derive the empirical correlations.

Variable temperature ^1H solid state MAS NMR experiments up to 195 °C show that all of the protons in $Ba_2In_2O_4(OH)_2$ are mobile on the NMR time scale, the resonances first broadening and then completely coalescing at around 150 °C, yielding a single site with an isotropic chemical shift of 4.4 ppm. Such a coalescence process occurs when the proton-hopping frequency k equals $\pi\Delta\nu/\sqrt{2}$ (where $\Delta\nu$ is the frequency separation between the peaks) indicating that the hopping rate between the two O2 environments (1.7 and 3.3 ppm) must be greater than $k \sim 2.2$ kHz, while that between the O1 and O2 sites is ~7 kHz (where shifts of 7.3 and 2.5 ppm are used in this calculation, 2.5 ppm being the predicted shift following coalescence of the 1.7 and 3.3 ppm resonances). As the

DOI: 10.1021/acs.chemmater.5b00328
Chem. Mater. 2015, 27, 3861–3873

temperature is increased further, the peak height of the new resonance increases as the line width narrows, due to an increase in proton motion. A weak resonance at 1.7 ppm persists even at 195 °C, this being assigned to both structures L (containing O2−H2 protons pointing to the O1 (bare) oxygens) and J (containing O2−H2 protons alternatively pointing to both O1 and O3 sites J). We suggest the O2−H1···O1 protons are more strongly trapped, while the O2−H1···O3 protons undergo more rapid exchange with the O3−H (H2) protons.

Two dimensional exchange NMR experiments were performed to explore motion on a longer time scale (Figure 9). Both chemical exchange and magnetization exchange (due to spin-diffusion) will result in cross-peaks situated off the ^{1}H vs ^{1}H diagonal. At 42 °C, cross-peaks are observed between the two distinct protons assigned to the O2 layer (H1; sites at 1.7 and 3.3 ppm) at a mixing time of 1 ms, indicating that these sites occur within a single particle. The cross-peaks are most likely generated from a combination of slow motion and spin diffusion. Longer mixing times reveal cross-peaks between all of the resonances, most likely as a result of spin diffusion. The observation of H1−H1 and H1−H2 cross-peaks at short mixing times (0.1 and 1 ms, respectively) at 80 °C is ascribed to the onset of motion, since the spin diffusion rates are unlikely to increase with temperature. At a temperature of 150 °C, all protons exchange rapidly at a rate in excess of 10 kHz, in agreement with the variable temperature ^{1}H spectra (Figure 8).

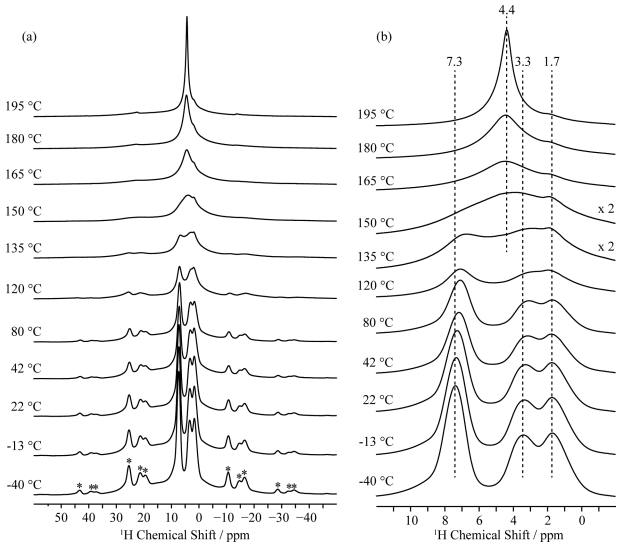

Figure 8. Variable temperature ^{1}H MAS NMR spectra of $Ba_2In_2O_4(OH)_2$ obtained at a MAS rate of 20 kHz and at 16.4 T. (a) Full spectral width showing the isotropic region and the spinning sideband manifold marked with asterisks. (b) Magnified view highlighting the coalescence of the 1.7 and 3.3 ppm resonances and coalescence of all the resonances above 150 °C.

The relatively rapid exchange between different proton sites at room temperature may seem inconsistent with the presence of multiple proton environments associated with excited states. However, the existence of some mobile protons does not necessarily imply that all of the protons can reorder into the unique ground state. Local orderings, even ones that allow significant H transport, could still be effectively locked in place as a cooperative ordering transition to the ground state could be inhibited, or some of the H could be immobile. The 2D

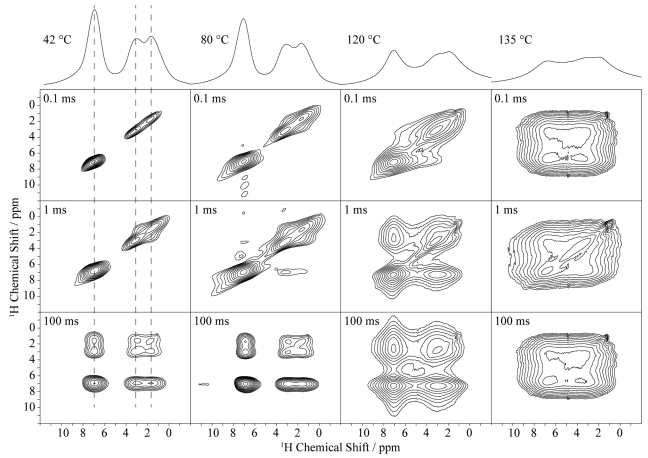

Figure 9. Variable temperature two-dimensional ^{1}H chemical exchange experiments as a function of mixing time, obtained at a MAS rate of 20 kHz and at 16.4 T. Only the isotropic region is shown. Single pulse 1D ^{1}H spectra (from Figure 8) are shown above the 2D plots.

spectra indicate that some of the proton configurations are present *within* the same particle. We indicated earlier that, within the errors of the DFT, no unique ground state structure emerges (ours differing from that of Martinez et al.[12]). Thus, it is likely that the lower energy structures reflect the different possible H-bonding configurations within one particle and that the four lowest structures identified in this study represent the more probable configurations. A future study treating the H ordering with a more complete thermodynamics and kinetic model would be valuable, but this is beyond the scope of this current work.

4. CONCLUSIONS

In summary, we have performed a comprehensive structural analysis of the hydrated form of brownmillerite, $Ba_2In_2O_4(OH)_2$, using multinuclear solid state NMR spectroscopy in combination with solid state DFT calculations. We reproduce the structural analysis of a large number of possible proton positions of Martinez et al.,[12] identifying multiple configurations that may exist concurrently at room temperature. Three different proton sites were observed by ^{1}H MAS NMR spectroscopy, which were found to exchange at 150 °C on the NMR time scale with hopping rates in excess of 10 kHz. Assignment of these resonances make use of extensive total energy DFT calculations of a wide range of proton configurations, which yielded four chemically similar low energy configurations, the simulated ^{1}H GIPAW NMR spectra of which are in relatively good agreement with the experimental data. The three resonances can be assigned as follows: the high frequency shift corresponds to O3 layer protons (H2), while the two lower frequency shifts arise due to two types of configurations of O2 layer protons (H1) with shorter and longer H···O (hydrogen bond) distances and a difference in O−H···O angles. Distinct O2 layer proton (H1) configurations are observed in four low energy structures that perhaps coexist at room temperature. The ^{17}O NMR spectrum of $Ba_2In_2O_4(OH)_2$ is dominated by four O sites, which can be rationalized by the DFT GIPAW calculations, which reveal that H-donor oxygens appear at lower shift while the nonhydroxyl oxygens and H-acceptor O are visible at higher shifts. We suggest that all the lower energy proton sites should be

DOI: 10.1021/acs.chemmater.5b00328
Chem. Mater. 2015, 27, 3861−3873

considered in any proposed proton conduction mechanism within the $Ba_2In_2O_4(OH)_2$ phase.

The joint experimental and theoretical approach presented in this work can be readily applied to investigate H-bonding and local structure in other hydrated perovskites. The current work suggests that multiple H-bonding motifs are likely present in related structures, the relative energies of these strongly affecting proton trapping and conductivity.

■ ASSOCIATED CONTENT

Supporting Information

X-ray diffraction patterns (Figure S1), TGA (Figure S2), plot of experimental isotropic shift, δ_{iso}, against computed isotropic shielding, σ_{iso}, for ^1H sites (Figure S3), two-dimensional $^1H-^{17}O$ CP HETCOR NMR spectrum and ^{17}O CP spectra with various contact times of $Ba_2In_2O_4(OH)_2$ (Figure S4), 17O CP kinetics graph (Figure S5), ^1H NMR spectrum of $Ba_2In_2O_4(OH)_2$ obtained under MAS rate of 60 kHz (Figure S6), GIPAW calculated ^1H NMR chemical shifts, δ_{iso}, of all structures investigated (Figure S7), and detailed representation of all configurations considered as optimized structures and complete GIPAW NMR data. The Supporting Information is available free of charge on the ACS Publications website at DOI: 10.1021/acs.chemmater.5b00328.

■ AUTHOR INFORMATION

Corresponding Author

*E-mail: cpg27@cam.ac.uk.

Present Addresses

[‖](R.D.) Institute for Molecules and Materials, Radboud University, P. O. Box 9010, 6500 GL, Nijmegen, The Netherlands.

[⊥](F.B.) Department of Chemistry and Stephenson Institute for Renewable Energy, University of Liverpool, Crown Street, Liverpool L69 7ZD, U.K.

Funding

This work was supported in part by Grants DMR050612 and CHE0714183 from the National Science Foundation and Grant DESC0001284 from the Department of Energy (supporting Y.-L.L. and D.M.), by an Advanced Fellowship from the EU-ERC (C.P.G.), and by the EPSRC (D.S.M.). F.B. thanks the EU Marie Curie actions FP7 for an International Incoming fellowship (Grant No. 275212) and Clare Hall, University of Cambridge, for a Research Fellowship.

Notes

The authors declare no competing financial interest.

■ ACKNOWLEDGMENTS

We thank Dr. Andrew J. Ilott (NYU, New York, NY, USA), Dr. Aurélie Rolle (University of Lille Nord de France, France), Dr. John M. Griffin (University of Cambridge, U.K.), and Dr. Gunwoo Kim (University of Cambridge, U.K.) for helpful discussions and Luke Sperrin (University of Cambridge, U.K.) for running the TGA experiments. Research was carried out in part at the Center for Functional Nanomaterials, Brookhaven National Laboratory, NY, USA, which is supported by the U.S. Department of Energy, Office of Basic Energy Sciences, under Contract No. DE-AC02-98CH10886.

■ ABBREVIATIONS

DFT, density functional theory; fwhm, full width at half-maximum; GIPAW, gauge including projector augmented wave; MAS, magic angle spinning; NMR, nuclear magnetic resonance

■ REFERENCES

(1) Ishihara, T.; Yokokawa, H.; Iwahara, H.; Kilner, J. A.; Berenov, A.; Rossiny, J.; Yashima, M.; Kawada, T.; Irvine, J. T. S.; Akbay, T.; Kawakami, A.; Norby, T.; Matsumoto, H.; Kreuer, K. D.; Ito, N.; Horita, T. *Perovskite Oxide for Solid Oxide Fuel Cells*; Springer: New York, 2009.

(2) Malavasi, L.; Fisher, C. A. J.; Islam, M. S. Oxide-ion and proton conducting electrolyte materials for clean energy applications: Structural and mechanistic features. *Chem. Soc. Rev.* **2010**, *39* (11), 4370−4387.

(3) Takahashi, T.; Iwahara, H. Solid-state ionics: Protonic conduction in perovskite type oxide solid solutions. *Rev. Chim. Miner.* **1980**, *17* (4), 243−253.

(4) Iwahara, H.; Esaka, T.; Uchida, H.; Maeda, N. Proton conduction in sintered oxides and its application to steam electrolysis for hydrogen production. *Solid State Ionics* **1981**, *3*−*4*, 359−363.

(5) Iwahara, H. High temperature proton conducting oxides and their applications to solid electrolyte fuel cells and steam electrolyzer for hydrogen production. *Solid State Ionics* **1988**, *28*−*30*, 573−578 (Part 1).

(6) Iwahara, H.; Uchida, H.; Morimoto, K.; Hosogi, S. High-temperature C_1-gas fuel cells using proton-conducting solid electrolytes. *J. Appl. Electrochem.* **1989**, *19* (3), 448−452.

(7) Iwahara, H.; Uchida, H.; Morimoto, K. High temperature solid electrolyte fuel cells using perovskite-type oxide based on $BaCeO_3$. *J. Electrochem. Soc.* **1990**, *137* (2), 462−465.

(8) Lee, W.-K.; Nowick, A. S.; Boatner, L. A. Protonic conduction in acceptor-doped $KTaO_3$ crystals. *Solid State Ionics* **1986**, *18*−*19*, 989−993 (Part 2).

(9) Liang, K. C.; Nowick, A. S. High-temperature protonic conduction in mixed perovskite ceramics. *Solid State Ionics* **1993**, *61* (1−3), 77−81.

(10) Liang, K. C.; Du, Y.; Nowick, A. S. Fast high-temperature proton transport in nonstoichiometric mixed perovskites. *Solid State Ionics* **1994**, *69* (2), 117−120.

(11) Jayaraman, V.; Magrez, A.; Caldes, M.; Joubert, O.; Taulelle, F.; Rodriguezcarvajal, J.; Piffard, Y.; Brohan, L. Characterization of perovskite systems derived from $Ba_2In_2O_5\square$ Part II: The proton compounds $Ba_2In_{2(1-x)}Ti_{2x}O_{4+2x}(OH)_y$ $[0 \le x \le 1; y \le 2(1-x)]$. *Solid State Ionics* **2004**, *170* (1−2), 25−32.

(12) Martinez, J.-R.; Mohn, C. E.; Stølen, S.; Allan, N. L. $Ba_2In_2O_4(OH)_2$: Proton sites, disorder and vibrational properties. *J. Solid State Chem.* **2007**, *180* (12), 3388−3392.

(13) Colville, A. A.; Geller, S. The crystal structure of brownmillerite, Ca_2FeAlO_5. *Acta Crystallogr. B* **1971**, *27*, 2311−2315.

(14) Kreuer, K. D. Proton-Conducting Oxides. *Annu. Rev. Mater. Res.* **2003**, *33*, 333−359.

(15) Cervera, R. B.; Miyoshi, S.; Oyama, Y.; Elammari, Y. E.; Yagi, T.; Yamaguchi, S. Perovskite-Structured $BaScO_2(OH)$ as a Novel Proton Conductor: Heavily Hydrated Phase Obtained via Low-Temperature Synthesis. *Chem. Mater.* **2013**, *25* (9), 1483−1489.

(16) Yildirim, T.; Reisner, B.; Udovic, T. J.; Neumann, D. A. The combined neutron scattering and first-principles study of solid state protonic conductors. *Solid State Ionics* **2001**, *145*, 429−435.

(17) Schober, T.; Friedrich, J.; Krug, F. Phase transition in the oxygen and proton conductor $Ba_2In_2O_5$ in humid atmospheres below 300 °C. *Solid State Ionics* **1997**, *99*, 9−13.

(18) Schober, T.; Friedrich, J. The oxygen and proton conductor $Ba_2In_2O_5$: Thermogravimetry of proton uptake. *Solid State Ionics* **1998**, *113*−*115*, 369−375.

(19) Fischer, W.; Reck, G.; Schober, T. Structural transformation of the oxygen and proton conductor $Ba_2In_2O_5$ in humid air: an in-situ X-ray powder diffraction study. *Solid State Ionics* **1999**, *116*, 211−215.

(20) Fisher, C. A. J.; Islam, M. S. Defect, protons and conductivity in brownmillerite-structured $Ba_2In_2O_5$. *Solid State Ionics* **1999**, *118*, 355−363.

DOI: 10.1021/acs.chemmater.5b00328
Chem. Mater. 2015, 27, 3861−3873

(21) Gregory, D. H.; Weller, M. T. Phases in the System $Ba_2M_{2-x}Cu_xO_{4+\delta}$, M = In, Sc: Structure and Oxygen Stoichiometry. *J. Solid State Chem.* **1993**, *107*, 134−148.
(22) Dervisoglu, R.; Middlemiss, D. S.; Blanc, F.; Holmes, L. A.; Lee, Y. L.; Morgan, D.; Grey, C. P. Joint experimental and computational ^{17}O solid state NMR study of Brownmillerite $Ba_2In_2O_5$. *Phys. Chem. Chem. Phys.* **2014**, *16* (6), 2597−2606.
(23) Zhang, G. B.; Smyth, D. M. Protonic conduction in $Ba_2In_2O_5$. *Solid State Ionics* **1995**, *82* (3−4), 153−160.
(24) Hahn, T. *International tables for crystallography*, 5th rev. ed.; International Union of Crystallography by Springer: Dordrecht, The Netherlands, 2005; Vol. *A*.
(25) Pickard, C.; Mauri, F. All-electron magnetic response with pseudopotentials: NMR chemical shifts. *Phys. Rev. B* **2001**, *63*, 1−13.
(26) Huo, H.; Peng, L.; Gan, Z.; Grey, C. P. Solid-State MAS NMR Studies of Brønsted Acid Sites in Zeolite H-Mordenite. *J. Am. Chem. Soc.* **2012**, *134* (23), 9708−9720.
(27) Peng, L.; Huo, H.; Liu, Y.; Grey, C. P. ^{17}O magic angle spinning NMR studies of Bronsted acid sites in zeolites HY and HZSM-5. *J. Am. Chem. Soc.* **2007**, *129* (2), 335−346.
(28) Hartmann, S. R.; Hahn, E. L. Nuclear Double Resonance in the Rotating Frame. *Phys. Rev.* **1962**, *128* (5), 2042−2053.
(29) Schaefer, J.; Stejskal, E. O. Carbon-13 nuclear magnetic resonance of polymers spinning at the magic angle. *J. Am. Chem. Soc.* **1976**, *98* (4), 1031−1032.
(30) Fung, B. M.; Khitrin, A. K.; Ermolaev, K. An Improved Broadband Decoupling Sequence for Liquid Crystals and Solids. *J. Magn. Reson.* **2000**, *142* (1), 97−101.
(31) Odedra, S.; Wimperis, S. Improved background suppression in ^1H MAS NMR using composite pulses. *J. Magn. Reson.* **2012**, *221*, 41−50.
(32) Bielecki, A.; Burum, D. P. Temperature Dependence of ^{207}Pb MAS Spectra of Solid Lead Nitrate. An Accurate, Sensitive Thermometer for Variable-Temperature MAS. *J. Magn. Reson., Ser. A* **1995**, *116*, 215−220.
(33) Beckmann, P.; Dybowski, C. A thermometer for nonspinning solid-state NMR spectroscopy. *J. Magn. Reson.* **2000**, *146*, 379−380.
(34) BRUKER. *Topspin 3.1, software for NMR spectral analysis*; Bruker Biospin: Rheinstetten, Germany, 2011.
(35) van Beek, J. D. matNMR: A flexible toolbox for processing, analyzing and visualizing magnetic resonance data in Matlab®. *J. Magn. Reson.* **2007**, *187* (1), 19−26.
(36) Bak, M.; Rasmussen, J. T.; Nielsen, N. C. SIMPSON: A General Simulation Program for Solid-State NMR Spectroscopy. *J. Magn. Reson.* **2000**, *147* (2), 296−330.
(37) Middlemiss, D. S.; Blanc, F.; Pickard, C. J.; Grey, C. P. Solid-state NMR calculations for metal oxides and gallates: shielding and quadrupolar parameters for perovskites and related phases. *J. Magn. Reson.* **2010**, *204* (1), 1−10.
(38) Blanc, F.; Middlemiss, D. S.; Gan, Z.; Grey, C. P. Defects in doped $LaGaO_3$ anionic conductors: Linking NMR spectral features, local environments, and defect thermodynamics. *J. Am. Chem. Soc.* **2011**, *133*, 17662−17672.
(39) Barrow, N. S.; Yates, J. R.; Feller, S. A.; Holland, D.; Ashbrook, S. E.; Hodgkinson, P.; Brown, S. P. Towards homonuclear J solid-state NMR correlation experiments for half-integer quadrupolar nuclei: Experimental and simulated ^{11}B MAS spin-echo dephasing and calculated 2J BB coupling constants for lithium diborate. *Phys. Chem. Chem. Phys.* **2011**, *13* (13), 5778−5789.
(40) Buannic, L.; Blanc, F.; Middlemiss, D. S.; Grey, C. P. Probing Cation and Vacancy Ordering in the Dry and Hydrated Yttrium-Substituted $BaSnO_3$ Perovskite by NMR Spectroscopy and First Principles Calculations: Implications for Proton Mobility. *J. Am. Chem. Soc.* **2012**, *134* (35), 14483−14498.
(41) Johnston, K. E.; Tang, C. C.; Parker, J. E.; Knight, K. S.; Lightfoot, P.; Ashbrook, S. E. The polar phase of $NaNbO_3$: A combined study by powder diffraction, solid-state NMR, and first-principles calculations. *J. Am. Chem. Soc.* **2010**, *132*, 8732−8746.
(42) Reader, S. W.; Mitchell, M. R.; Johnston, K. E.; Pickard, C. J.; Whittle, K. R.; Ashbrook, S. E. Cation Disorder in Pyrochlore Ceramics: ^{89}Y MAS NMR and First-Principles Calculations. *J. Phys. Chem. C* **2009**, *113* (43), 18874−18883.
(43) Mitchell, M. R.; Reader, S. W.; Johnston, K. E.; Pickard, C. J.; Whittle, K. R.; Ashbrook, S. E. ^{119}Sn MAS NMR and first-principles calculations for the investigation of disorder in stannate pyrochlores. *Phys. Chem. Chem. Phys.* **2011**, *13* (2), 488−497.
(44) Clark, S. J.; Segall, M. D.; Pickard, C. J.; Hasnip, P. J.; Probert, M. I. J.; Refson, K.; Payne, M. C. First principles methods using CASTEP. *Z. Kristallogr.* **2005**, *220*, 567−570.
(45) Perdew, J. P.; Burke, K.; Ernzerhof, M. Generalized Gradient Approximation Made Simple. *Phys. Rev. Lett.* **1996**, *77* (18), 3865−3868.
(46) Pinney, N.; Morgan, D. Ab initio study of structurally bound water at cation vacancy sites in Fe- and Al-oxyhydroxide materials. *Geochim. Cosmochim. Acta* **2013**, *114*, 94−111.
(47) Pinney, N.; Morgan, D. Thermodynamics of Al-substitution in Fe-oxyhydroxides. *Geochim. Cosmochim. Acta* **2013**, *120*, 514−530.
(48) Momma, K.; Izumi, F. VESTA: A three-dimensional visualization system for electronic and structural analysis. *J. Appl. Crystallogr.* **2008**, *41* (3), 653−658.
(49) Yates, J.; Pickard, C.; Mauri, F. Calculation of NMR chemical shifts for extended systems using ultrasoft pseudopotentials. *Phys. Rev. B* **2007**, *76*, 1−11.
(50) Profeta, M.; Mauri, F.; Pickard, C. J. Accurate first principles prediction of ^{17}O NMR parameters in SiO_2: Assignment of the zeolite ferrierite spectrum. *J. Am. Chem. Soc.* **2003**, *125*, 541−548.
(51) Sears, R. E. J.; Kaliaperumal, R.; Manogaran, S. ^1H shielding anisotropy in $Mg(OH)_2$: The isolated OH^- group. *J. Chem. Phys.* **1988**, *88* (4), 2284−2288.
(52) Yates, J. R.; Pham, T. N.; Pickard, C. J.; Mauri, F.; Amado, A. M.; Gil, A. M.; Brown, S. P. An Investigation of Weak CH···O Hydrogen Bonds in Maltose Anomers by a Combination of Calculation and Experimental Solid-State NMR Spectroscopy. *J. Am. Chem. Soc.* **2005**, *127* (29), 10216−10220.
(53) Webber, A. L.; Elena, B.; Griffin, J. M.; Yates, J. R.; Pham, T. N.; Mauri, F.; Pickard, C. J.; Gil, A. M.; Stein, R.; Lesage, A.; Emsley, L.; Brown, S. P. Complete ^1H resonance assignment of beta-maltose from ^1H-^1H DQ-SQ CRAMPS and ^1H (DQ-DUMBO)-^{13}C SQ refocused INEPT 2D solid-state NMR spectra and first principles GIPAW calculations. *Phys. Chem. Chem. Phys.* **2010**, *12*, 6970−6983.
(54) Sardo, M.; Siegel, R.; Santos, S. M.; Rocha, J.; Gomes, J. R. B.; Mafra, L. Combining multinuclear high-resolution solid-state MAS NMR and computational methods for resonance assignment of glutathione tripeptide. *J. Phys. Chem. A* **2012**, *116*, 6711−6719.
(55) Pyykkö, P. Year-2008 nuclear quadrupole moments. *Mol. Phys.* **2008**, *106* (16−18), 1965−1974.
(56) Jayaraman, V.; Magrez, A.; Caldes, M.; Joubert, O.; Ganne, M.; Piffard, Y.; Brohan, L. Characterization of perovskite systems derived from $Ba_2In_2O_5\square$ Part I: The oxygen-deficient $Ba_2In_{2(1-x)}Ti_{2x}O_{5+x}\square_{1-x}$ ($0 \le x \le 1$) compounds. *Solid State Ionics* **2004**, *170* (1−2), 17−24.
(57) Bielecki, J.; Parker, S. F.; Ekanayake, D.; Rahman, S. M. H.; Borjesson, L.; Karlsson, M. Short-range structure of the brownmillerite-type oxide $Ba_2In_2O_5$ and its hydrated proton-conducting form $BaInO_3H$. *J. Mater. Chem. A* **2014**, *2* (40), 16915−16924.
(58) Smith, M. E.; van Eck, E. R. H. Recent advances in experimental solid state NMR methodology for half-integer spin quadrupolar nuclei. *Prog. Nucl. Magn. Reson. Spectrosc.* **1999**, *34* (2), 159−201.
(59) Lesage, A. Recent advances in solid-state NMR spectroscopy of spin I = 1/2 nuclei. *Phys. Chem. Chem. Phys.* **2009**, *11* (32), 6876−6891.
(60) Yesinowski, J. P.; Eckert, H.; Rossman, G. R. Characterization of hydrous species in minerals by high-speed ^1H MAS-NMR. *J. Am. Chem. Soc.* **1988**, *110* (5), 1367−1375.
(61) Xue, X.; Kanzaki, M. Proton Distributions and Hydrogen Bonding in Crystalline and Glassy Hydrous Silicates and Related Inorganic Materials: Insights from High-Resolution Solid-State

DOI: 10.1021/acs.chemmater.5b00328
Chem. Mater. 2015, 27, 3861−3873

Nuclear Magnetic Resonance Spectroscopy. *J. Am. Ceram. Soc.* **2009**, *92* (12), 2803−2830.

DOI: 10.1021/acs.chemmater.5b00328
Chem. Mater. 2015, 27, 3861−3873